Accepted Manuscript

Title: Interfacial bonding mechanism in Al/coated steel dissimilar refill friction stir spot welds

Authors: Z. Shen, Y. Ding, J. Chen, B. Shalchi Amirkhiz, J.Z. Wen, L. Fu, A.P. Gerlich

PII: S1005-0302(19)30010-6
DOI: https://doi.org/10.1016/j.jmst.2019.01.001
Reference: JMST 1452

To appear in:

Received date: 23 February 2018
Revised date: 14 April 2018
Accepted date: 11 October 2018

Please cite this article as: Shen Z, Ding Y, Chen J, Shalchi Amirkhiz B, Wen JZ, Fu L, Gerlich AP, Interfacial bonding mechanism in Al/coated steel dissimilar refill friction stir spot welds, *Journal of Materials Science and amp; Technology* (2019), https://doi.org/10.1016/j.jmst.2019.01.001

Interfacial bonding mechanism in Al/coated steel dissimilar refill friction stir spot welds

Z. Shen [a, b, c, *], Y. Ding [c], J. Chen [d, *], B. Shalchi Amirkhiz [d], J.Z. Wen [c], L. Fu [a, b], A.P. Gerlich [c]

[a] State Key Laboratory of Solidification Processing, Northwestern Polytechnical University, Xi'an 710072, China

[b] Shanxi Key Laboratory of Friction Welding Technologies, Northwestern Polytechnical University, Xi'an 710072, China

[c] Department of Mechanical and Mechatronics Engineering, University of Waterloo, Waterloo N2L 3G1, Canada

[d] CanmetMATERIALS, Natural Resources Canada, Hamilton L8P 0A5, Canada

* Corresponding authors.
E-mail addresses: z45shen@uwaterloo.ca (Z. Shen), jameszheng.chen@canada.ca (J. Chen).

[Received 23 February 2018; revised 14 April 2018; accepted 11 October 2018]

Abstract

Defect-free dissimilar Al/zinc coated steel and Al/AlSi coated steel welds were successfully fabricated by refill friction stir spot welding. However, Al alloy and uncoated steel could not be welded under the same welding condition. Al-Zn eutectic layer formed at the Al/zinc coated steel interface showed non-uniformity in thickness and nanoscale intermetallic (IMC) produced was discontinuous. The bonding formation between the Al-Zn layer and the surrounding materials was attributed to a liquid/solid reaction mechanism. Bonding formation at Al alloy and AlSi coated steel interface was attributed to a solid/solid reaction mechanism, as the joining process did not involve with melting of base metals or AlSi coating materials. Kissing bond formed at the weld boundary acted as a crack initiation and propagation site, and the present study showed that weld strength of Al 5754/AlSi coated steel was greatly influenced by properties of original IMC layer.

Keywords: Refill friction stir spot welding, Al alloy, Steel, Coated materials, Joining mechanism.

1. Introduction

Al alloys provide low density and excellent corrosion resistance, steels are mainly selected for contributing cost-effective strength and high stiffness. Dissimilar joining Al alloys to steels is an effective method to combine the attractive property profiles of these most common structural materials in one hybrid part [1]. Currently, there are two major approaches to join Al alloys to steels, which are mechanical joining such as self-piercing rivets and clinching [2, 3], and metallurgical joining such

as fusion and solid-state joining technologies [4-8]. The mechanical joining technologies introduce use of fasteners such as screws or rivets, which increases the cost and structure weight. Fusion joining technologies are problematic since they could result in formation of bulk intermetallic compounds (IMCs) at elevated temperatures [9]. These IMCs are brittle, and a thick or continuous IMC layer severely deteriorates the weld strength [10].

Conventional friction stir spot welding (FSSW) is a relatively new solid-state joining technology, which is a natural alternative to fusion welding due to that it avoids the problems of solidification and liquation cracking [11-29]. Mazda has used conventional FSSW to join Al alloy to coated steels in aluminum trunk lid [27], acceptable weld strength was achieved although keyhole significantly decreased effective bonded area [11-15]. There are three main approaches of joining Al alloy to steel by conventional FSSW: (i) directly joining Al to uncoated steel through the formation of IMCs while avoiding plunging the tool pin into bottom steels [11-16], (ii) mechanical interlocking by displacing the bottom steel into the Al sheet [17-23], and (iii) adoption of coatings on steels to promote the interfacial bonding [24-28]. It is noted that a relatively longer welding cycle (5-15 s) needs to be applied to promote the IMCs layer formation when directly joining Al to uncoated steels [11, 12, 14], which is impractical for the mass production. Meanwhile, advanced tool material such as WC–Co [19], WC [20, 22], W25Re [17, 18, 21], tungsten carbide [22], or silicon nitride should be used to obtain interlocking mechanism by plunging tool pin into the bottom steels [23].

Refill FSSW, a new solid-state joining technology developed by Schilling et al. in Helmholtz-Zentrum Geesthacht (HZG, former GKSS) [30], showed great advantages comparing to conventional FSSW as refill FSSW could significantly increase effective weld area and weld strength [31-33]. Refill FSSW process has been described in detail in the prior literature, and successfully applied to join lightweight materials [32, 34-37], and dissimilar metals [38-46]. Al/steel dissimilar refill friction stir spot weld strength is much higher than conventional FSSW due to the larger bonded area and preferable improved weld integrity [39, 42, 44]. Given the large discrepancies in physical and chemical properties between Al and Fe, it is rather challenging to directly join Al alloys to steels [47, 48]. Furthermore, it is impractical to plunge expensive steel tool into harder bottom steels to obtain the mechanical interlocking. According to the literature available, joining Al alloys to steels by refill FSSW consistently involves adoption of coatings on steel for promoting interfacial bonding, while avoiding plunging the tool into the bottom steels. Excellent weld strength can be achieved by pure metallurgical joining mechanism [39-44]. In this case, condition of material contact surface plays a crucial role in determining interfacial microstructure and weld strength [39, 40].

Galvanizing and aluminizing are the two most commonly used processing techniques for protecting steel components exposed to corrosive and oxidic environments [49-51]. Coated material has a pronounced influence on the joining

mechanisms due to differences in physical and chemical properties [26], which it acts as a filler material between materials to be joined [39], preventing direct contact of Al and Fe and thus formation of bulk IMCs. Fukada et al. first reported the feasibility of joining Al alloy to zinc-coated steel by refill FSSW, it was found that IMC layer in some micro mater thickness was not observed at the Al/steel interface, and the weld strength exceeded JIS standard value for RSW [43]. More recently, Shen et al. reported that presence of zinc coating promoted formation of Al-Zn eutectic structure layer, with generation of an additional brazing effect out of sleeve periphery [39]. Ding et al. demonstrated that strong bonding was achieved between Al alloy and AlSi coated steel, with weld strength showed less sensitivity to welding parameters than Al/zinc coated weld [40]. It would be worthwhile to clarify effect of coated material on interfacial joining mechanism since the crack mainly propagated along the Al/steel interface [26, 39-44, 46]. Therefore, Al 6022 was used to join to uncoated and zinc coated DP600 steels, and Al 5754 was used to join to AlSi coated steel by refill FSSW, interfacial microstructure and joining mechanisms were obtained.

2. Experimental procedures

Top Al alloys used in the present study were 1.6 mm thick Al 6022-T4 and Al 5754-O, and the bottom steels were 2.0 mm thick zinc coated DP600 steel and AlSi coated Usibor 1500P steel (or 22MnB5 alloy) [39, 40]. For direct-comparison, 2.0 mm thick uncoated DP600 steel was selected as experimental materials. Al in small quantity has been generally applied into zinc bath for slowing down reaction rate of zinc-iron, due to the role of inhibition of Al [51]. Approximately 10 wt. % silicon can be applied as an added element in aluminum bath to minimize the IMC thickness and flatten interface between IMC layer and steel substrate [50, 52, 53]. Chemical compositions of the Al alloys, steel substrates and the coated materials are listed in Table. 1. As shown in Fig. 1, grain size of Al 6022 sheet material was approx. 79 μm with precipitates β-Mg_2Si at grain boundaries [54]. Zinc coating thickness on the DP600 steel substrate is approx. 10 μm, while the coating on the boron steel is comprised of a 18.5 μm thick AlSi eutectic layer and a 9.5 μm thick ununiform IMC layer, the IMC layer is identified to be a 8.5 μm thick Al_7Fe_2Si and a 1.0 μm thick $Al_5Fe_2(Si)$ [40].

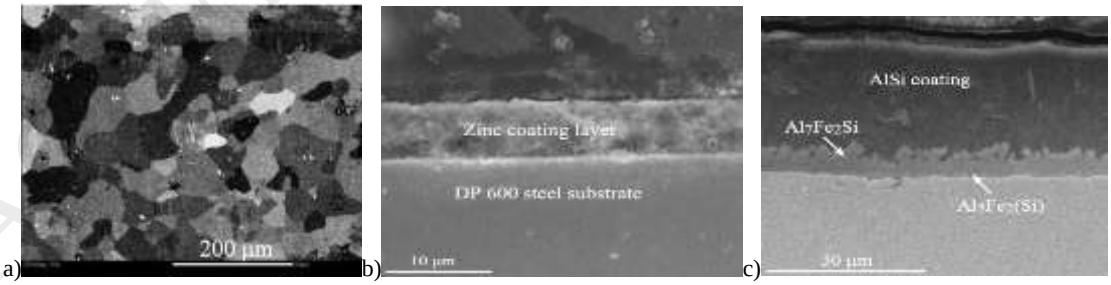

Fig. 1. Microstructure of as-received base metals: (a) Al 6022-T4, (b) Zinc coated DP600 steel and (c) AlSi coated Usibor 1500P steel (or 22MnB5 alloy).

Table. 1. Chemical compositions of as-received materials and coated materials (wt%) [39, 40].

Materials	Al	Fe	Si	Zn	Cr	Mg	Mn	B	Cu	P	Ti	C	S	Cr+Mo+Ni
Al 6022	Bal.	0.05-0.20	0.80-1.5	<0.25	0.1	0.07-0.45	0.02-0.10		0.01-0.11		<0.15			
Al 5754	Bal.	0.4	0.4			2.6-3.2	0.5							
DP600		Bal.	1.5				2			0.04		0.14	0.015	1
22MnB5	0.03	Bal.	0.015		0.16		2.2	0.004		0.02	0.035	0.22		
Zn coating	0.3	2.0		97.7										
AlSi coating	86.2	1.3	12.5											

Fig. 2 schematically shows the joining steps applied in the present study, in which the tool did not plunge into the bottom steel during the entire joining process of the study. Diameters of clamping ring, sleeve and pin were 14.5, 9.0 and 6.4 mm, respectively. Al 6022/uncoated DP600 steel and Al 6022/zinc coated DP600 welds were manufactured using a rotational speed of 1800 rpm, a tool sleeve penetration depth of 1.0 mm and a welding time of 3.707 s [39]. The Al 5754/AlSi coated steel welds were manufactured using a rotational speed of 2800 rpm, a penetration time of 0.5 s, a dwell time of 3.5 s and a retraction time of 0.5 s, which are constant during the welding process. Since penetration depth into upper Al 5754 varied from 0.9 to 1.4 mm, plunging (retreating) rate had therefore varied adjusted with variation of 1.8 to 2.8 mm/s. Prior to welding process, the base metals were sanitized with ethanol to remove impurities on surface. In reference to American Welding Society (AWS) standard D8.22M:2007 [55], the welds were fabricated by applying 30 mm × 100 mm coupons with a 30 mm × 30 mm overlap area, and all specimens were welded in center of the overlapped area. As shown in Fig. 2(e), a K type thermocouple was inserted to the Al 5754/AlSi coated steel weld boundary through the groove cut on the bottom steel sheet to record thermal cycle. Tool current, rotational speed and penetration were recorded by using a M-Scope software.

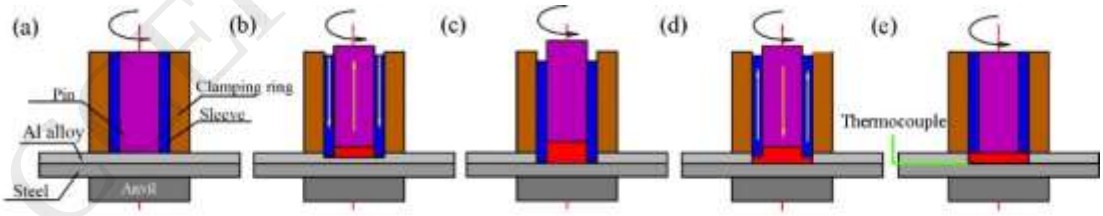

Fig. 2. Schematic representation of refill FSSW process: (a) surface preheating while clamping and spindles rotation, (b) sleeve plunges into the sheets while pin moves upwards, (c) tool dwells at a predetermined penetration depth, d) spindles retract back, and (e) surface dwell to flatten the weld surface.

At completion of welding, the weld was sectioned at weld center, which it was conducted using standard metallographic techniques with final polishing using 1 μm

diamond abrasive. Weld microstructure was observed using an OLYMPUS NTB 3558 optical microscope, and a JEOL JSM-6460 scanning electron microscope (SEM) with 20 kV operating voltage equipped with ENCA 3.5 energy dispersive X-ray (EDX) analysis system. Chemical compositions measured by EDX spectroscopy were reported as wt%. Transmission electron microscopy (TEM) study was conducted using FEI's Tecnai Osiris TEM equipped with X-FEG gun at 200 kV. To study phase identification and crystallography of weld materials, bright field, dark field imaging, selected area diffraction (SAD) technique were used. Scanning transmission electron microscopy (STEM) mode using bright field (BF) and high angle annular dark field (HAADF) detectors were applied in combination with EDX. The hardness distribution was measured at the mid-thickness of the top Al 6022 and Al 5754 sheets with a load of 50 gf and a dwell time of 10 s. The lap shear testing was performed at a constant cross head speed of 10 mm/min.

3. Results and discussion

3.1. Joining of Al alloy to uncoated steels

Firstly, the Al 6022 sheet was used to join to uncoated DP600 steel to study the feasibility of directly joining Al alloy to uncoated steels. As shown in Fig. 3, effective interfacial bonding cannot be achieved between Al 6022 and the uncoated steel by using the same welding condition as joining Al 6022 to zinc coated steels. Top Al 6022 and the bottom steel separated directly at completion of the joining process. Oxide films on surfaces of the coupon were unable to broken down into particles due to insufficient temperature and axial force imposed by welding tool. Macro plastic deformation was not observed at the interfacial center, because pin was not plunged into top Al 6022 material during the entire joining process. However, a small quantity of Al sheet materials was found to attach on the bottom steels at interfacial boundary area, which suggests occurrence of interfacial reaction between Al and Fe at the localized regions, regardless of a small reaction area that unable to promote effective bonding.

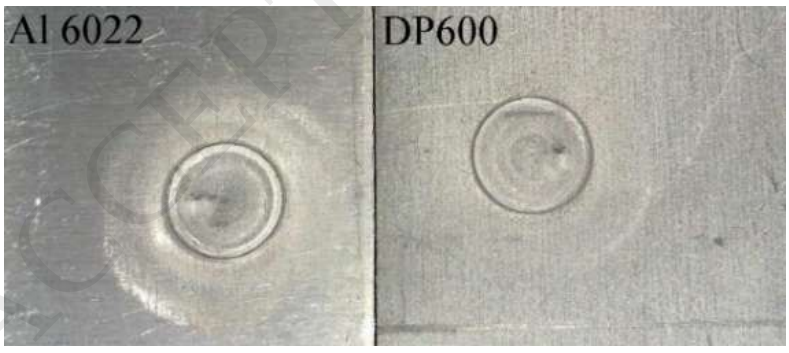

Fig. 3. Macroscopic appearance of two unbonded two surfaces on Al and steel sides, respectively.

3.2. Interfacial microstructure of Al/zinc coated steel weld

In similarity with joining Al alloy to zinc coated steel using friction stir lap

welding [48], present study shows that the presence of zinc coating could significantly improve the weldability of Al alloy and steels. Fig. 4(a) shows a representative macroscopic view of Al 6022/zinc coated DP600 steel weld, which was produced using a rotational speed of 1800 rpm and 1.0 mm penetration depth. The sleeve plunge path was indicated by the black dash-dotted line, the weld was completely refilled, with no defects could be observed through the weld. Top surface of the weld showed a slightly higher position than original surface of Al 6022 due to the impact of axial force, which was imposed by clamp ring. It also suggests that there was no material loss during welding process. The Al/steel interface of weld was uniform, where no defects such as voids or cracking were detected. The observation was due to the production of weld was under an appropriate heat input welding condition in comparison to previous studies, thereby zinc coating material did not displaced into the top Al alloy [39].

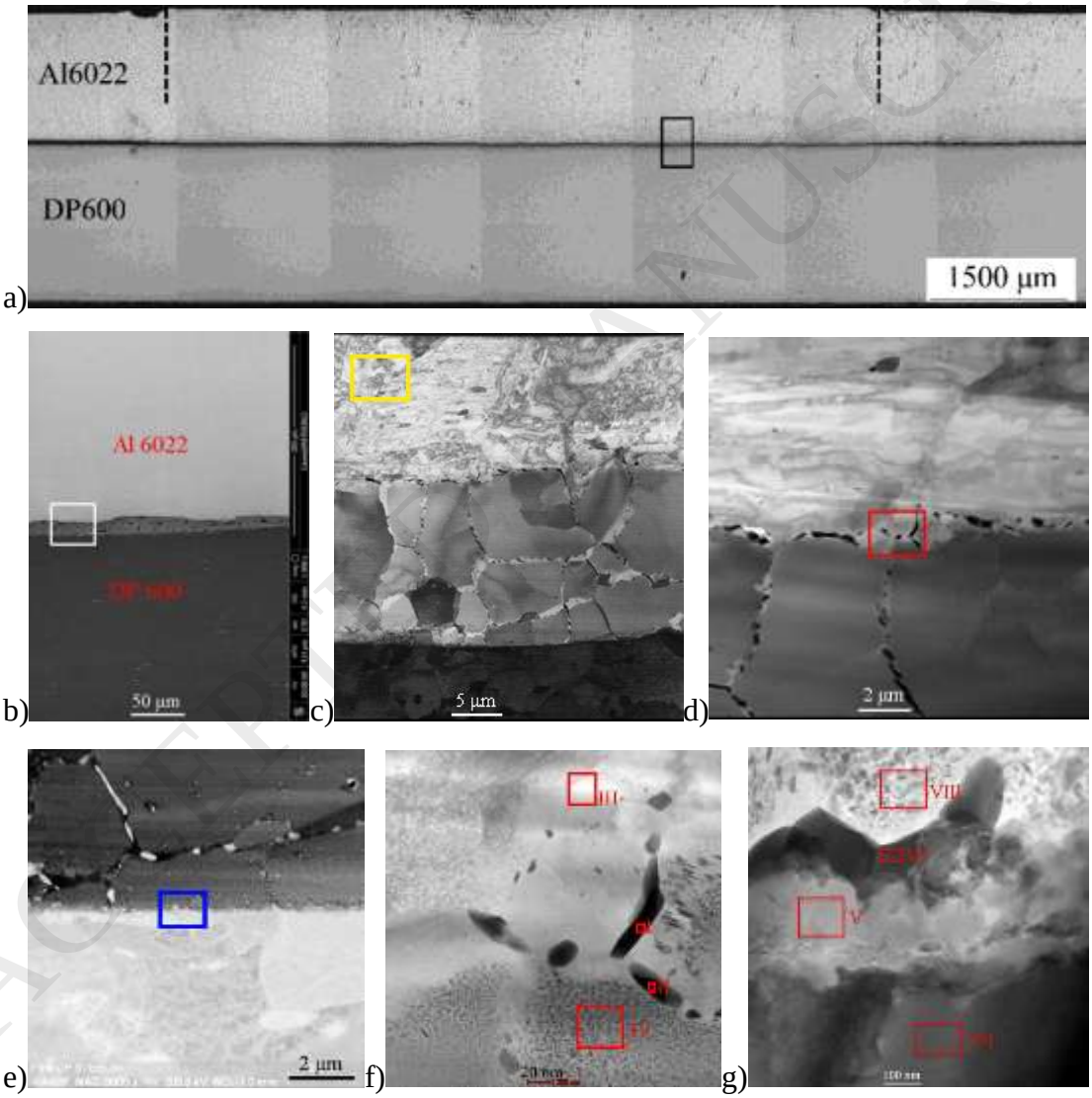

Fig. 4. (a) Cross section of the Al 6022/DP600 weld, (b) SEM image of magnified view of black rectangle in (a), STEM images in (c) magnified view of white rectangle in (b), (d) Al/Al-Zn layer interface, (e) Al-Zn layer/steel interface, (f) magnified view of red rectangle in (d), and (g) magnified view of blue rectangle in (e).

Magnified view of black rectangle in Fig. 4(a) is shown in Fig. 4(b), liquid state inter-diffusion between Al and zinc coating material produced an Al-Zn eutectic structure layer at the Al/steel interface, as the temperature at the interface exceeded Al–Zn eutectic point of 381°C [39]. Distribution of the Al-Zn layer was inhomogeneous due to a complex material flow pattern in the stir zone. As demonstrated by Fig. 4(c), which shows magnified view of white rectangle in Fig. 4(b), Al-Zn solid solution structure was characterized by refined and equiaxed grains, which it could probably attributed to occurrence of dynamic recrystallization generated by frictional heat and severe plastic deformation imposed by welding tool.

Images of interfaces at Al/Al-Zn layer and Al-Zn layer/steel of cross-section of the Al 6022/DP600 weld are shown in Fig. 4(d) and (e), respectively. The Al-Zn eutectic structure layer was well bonded to the top Al alloy materials and the bottom steel substrate, with no defects such as cracking or poles were observed at these interfaces. Sub-grain boundaries were noted within the Al-Zn eutectic structure grains (Fig. 4(d)), and this may be explained by plastic deformation and recovery throughout the welding process. The presence of sub-grain boundary is considered as beneficial to increase the weld strength because it can retard the movement of dislocation. Magnified views of red rectangle in Fig. 4(d) and blue rectangle in Fig. 4(e) were shown in Fig. 4(f) and (g), respectively. The chemical compositions in the regions I-VIII in are quantified in Table 2. As shown in Fig. 4(f-g) and Table. 2, the dark and white precipitates generated at the Al-Zn grain boundary have been identified as Zn-rich (regions I and II in Fig. 4(f), and region VI in Fig. 4(g)) and Al-rich (region III in Fig. 4(f)) phase particles, which their formation was associated with the eutectic reaction between Al and Zn.

Table. 2. EDX quantification results (wt%) indicated in Fig. 4(f) and (g).

	I	II	III	IV	V	VI	VII	VIII
Fe		0.1		0.1	37.8	1.1	100	0.6
Al	5.8	7.01	92.2	65.3	43.6	1.2		66.2
Zn	94.2	92.8	7.5	34.4	12.2	97.7		33.2
Si		0.1	0.3	0.2	6.4			

Fig. 5 shows hardness distribution measured through the mid-thickness of the top Al 6022 sheet. As a heat treatable alloy, a significant soft weld zone was generated in the Al 6022 due to a thermal cycle induced by the refill FSSW process, which it in turns could be attributed to the coarsening or dissolution of β-Mg_2Si [34]. Given the only impact of thermal cycle in heat affected zone (HAZ) was to form coarse grain size and coarsening / dissolution of precipitates, minimum hardness can be noted at the periphery between HAZ and thermos-mechanically affected zone (TMAZ). The hardness of Al 6022 was slightly increased in stir zone (SZ) due to formation of fine grain size, which was resulted by dynamic recrystallization.

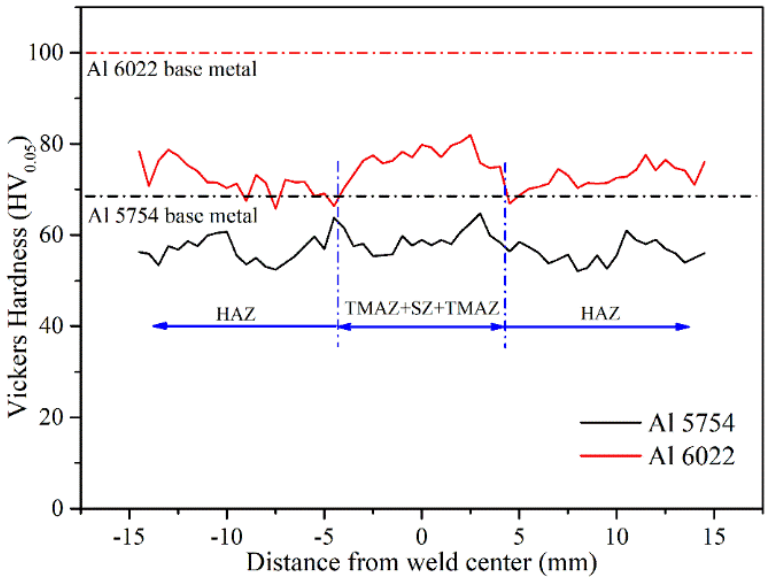

Fig. 5. Hardness distribution in middle-thickness of the top Al 6022 and Al 5754.

Fig. 6 shows the bright field images (TEM) and the corresponding SAD patterns of the selected areas at (a) Al side, which its magnified view is shown as yellow rectangle in Fig. 4(c), (b) Al-Zn eutectic structure and (c) zinc rich precipitate at the grain boundary. In Figs. 4(d) and 6(a), a highly deformed structure was very pronounced with Al 6022 material between the solid Al 6022 stir zone and the liquid Al-Zn eutectic structure. The deformed structure was elongated along the horizontal direction due to the impact of axial force imposed by welding tool and a pattern that was indexed as a [101] zone axis. The grain appearance was comparable to thermos-mechanically affected zone [34], however a significant finer grain size (≤ 1 μm in thickness) is shown than in the Al 6022 base metal (see Fig. 1(a)). The phenomenon could be explained by the occurrence of incomplete or discontinued dynamic recrystallization. As shown in Fig. 4(f) and Table. 2, Al-Zn eutectic structure is composed of 65.3%Al, 34.4%Zn, and low levels of Fe and Si, which presents a nanocrystalline structure with a [0 0 1] zone axis (see Fig. 6(b)), while the Zn-rich precipitate was indexed as a [3 6 2] zone axis (see Fig. 6(c)).

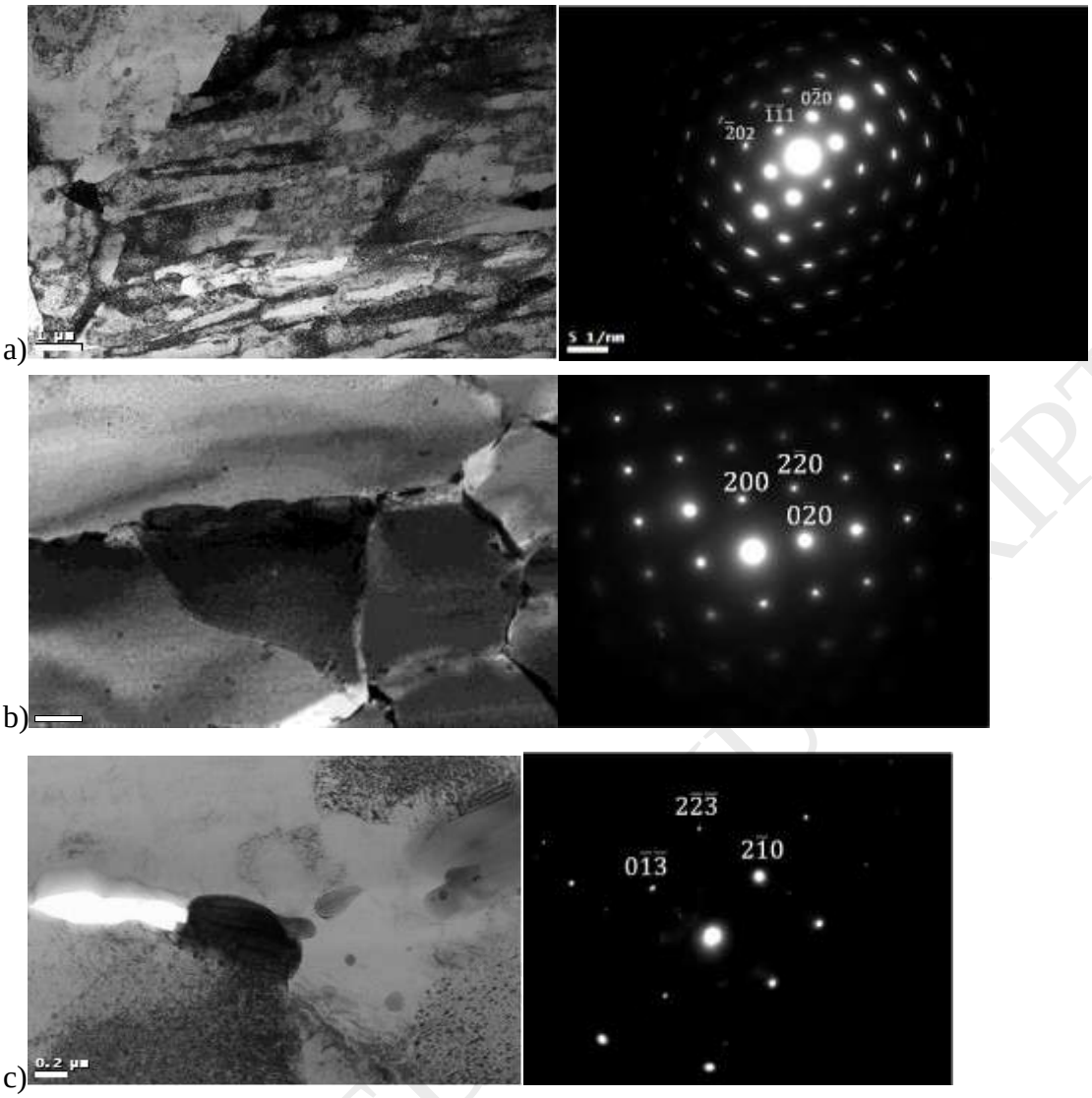

Fig. 6. Bright field images (TEM) and the corresponding SAD patterns of selected area at (a) Al side (magnified view of yellow rectangle as shown in Fig. 4(c)), (b) Al-Zn eutectic structure and (c) zinc rich precipitate at Al-Zn grain boundary.

In Fig. 4(e) and (g), intimate bonding was formed at Al-Zn layer/steel substrate interface due to a liquid/solid reaction, and element maps for Fe, Al, Si and Zn at the two locations are shown in Fig. 7(a) and (b), respectively. In Fig. 7(a), a high concentration level of Si was observed at the Al-Zn layer/steel substrate interface, indicating that the material was originated from the substrate materials. In addition to the nanoscale IMCs of Fe_4Al_{13} and FeAl [39], presence of Si at a high concentration level could have promoted the formation of nonuniform intermetallic layer, which shows amorphous or nanocrystalline structure (see Fig. 7(c)). Thickness of the IMCs layer is rather thin (< 200 nm), it is because that the presence of zinc coating could have prevented a direct contact between Al and steel, thereby inhibiting chemical reaction and interdiffusion. Furthermore, addition of silicon to aluminum has a retarding effect on the growth kinetics of reaction layers, although the growth suppression mechanism remains unclear [56, 57].

a) 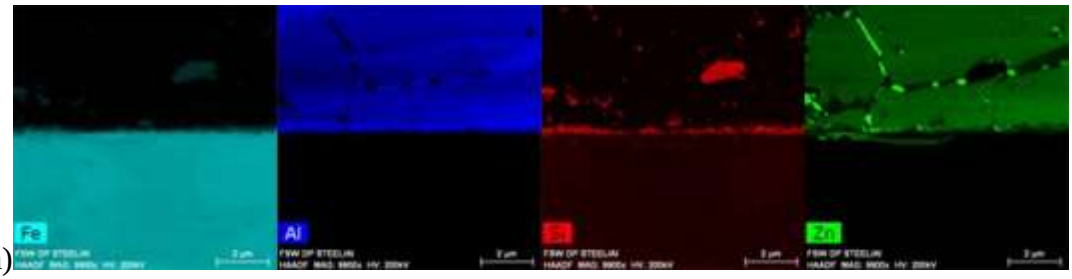

b) 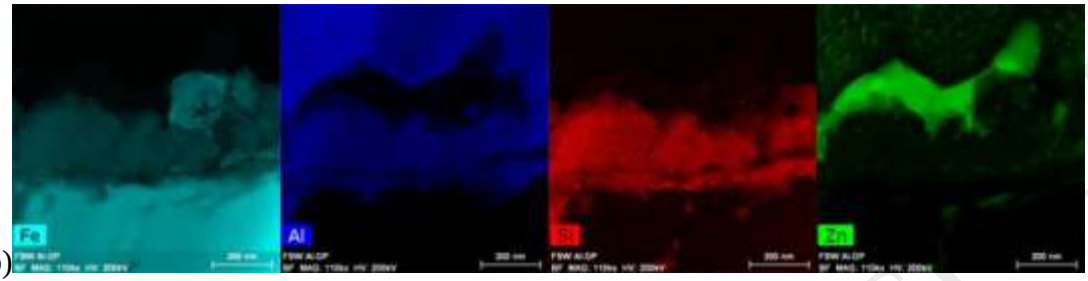

c) 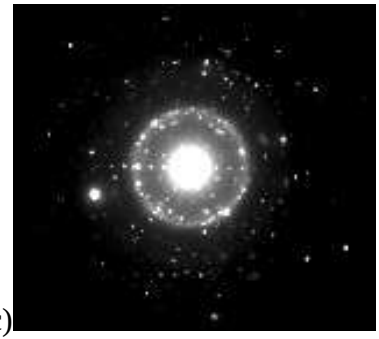

Fig. 7. Element maps of Fe, Al, Si and Zn in the Al-Zn layer/steel substrate interface at locations of (a) Fig. 4(e) and (b) Fig. 4(g), (c) SAD pattern of (a) region V in Fig. 4(g).

3.3. Interfacial joining mechanism of Al/AlSi coated steel weld

3.3.1. Heat generation and thermal cycle

Fig. 8 shows welding parameters (sleeve and pin positions, rotation speed) and tool current over welding time during refill FSSW of Al 5754 and AlSi coated steel. Real joining process started when the tool accelerated to a predetermined rotational condition at 2800 rpm from free running speed of 500 rpm within 0.5 s. In the meanwhile, rotational speed reduced again to the free running speed of 500 rpm after the sleeve and pin move back to the home position (workpiece surface). The tool rotational speed was maintained at a constant level during entire joining process, and the tool sleeve and pin position remained identical during the dwell period. It is noteworthy to mention that the pin moved further and faster than the sleeve due to a larger volume of sleeve.

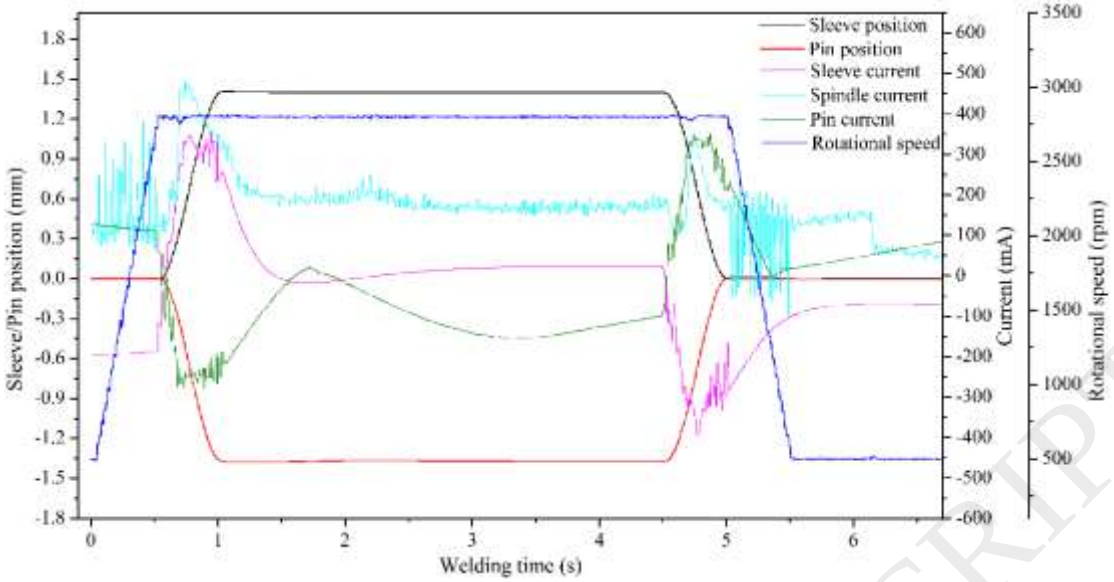

Fig. 8. Tool rotational speed, position and current during welding process.

According to Su and Gerlich et al. [58], the heat generation depends on tool axial force and torque:

$$Q_{applied} = \sum_{n=1}^{n=N} Force(n)(x_n - x_{n-1}) + \sum_{n=1}^{n=N} Torque\,(n)\omega(n), \Delta t$$

where x_n is the penetration depth at sample (n), ω is the angular velocity (rad s^{-1}), n is the sample number, N is the final sample and Δt is the sampling time.

In the present study, as shown in Fig. 8, the tool axial force is corresponding to both pin current and sleeve current, and the tool torque is corresponding to the spindle current. It is noted that tool torque was generated from the friction between each component of the tool [39], and axial force was generated from the tool frictional and relative motions (resulted from the tool vibration) during the tool rotational speed acceleration phase. Both the tool axial force and torque significantly increased during the tool sleeve penetration period, which could be attributed to the increase of strain rate and axial force. It is worth noting that the tool axial force sharply dropped during the dwell period, while the spindle current maintained at a constant level, which it probably because Al 5754 melting phenomena had not been involved in the dwelling process. In this regard, in comparison to tool penetration, tool rotation is a more significant factor influencing heat generation, the findings are also in agreement with the previous research [58-60].

Effect of tool penetration depth on thermal cycle at the Al 5754/AlSi coated steel interface is shown in Fig. 9. It is noted that interfacial temperature rapidly increased with increasing depth of tool sleeve penetration. Nonetheless, it was further observed that heating rate was not affected by the plunge rate, as heating rate during the tool penetration stage was determined by the tool rotational speed employed [60, 61]. Meanwhile, a higher extent of material was involved and stirred with increasing of penetration depth, which counteracts contribution of a higher plunging rate. The

temperature slightly dropped initially but gradually increased during the dwell period due to the impact of tool torque only (see Fig. 8) and this is because that the maximum temperature (482 ℃) did not exceed the solidus temperature of Al 5754 (590 ℃). In subsequent, the temperature dropped at a relatively lower cooling rate when the spot weld cooled to room temperature following welding.

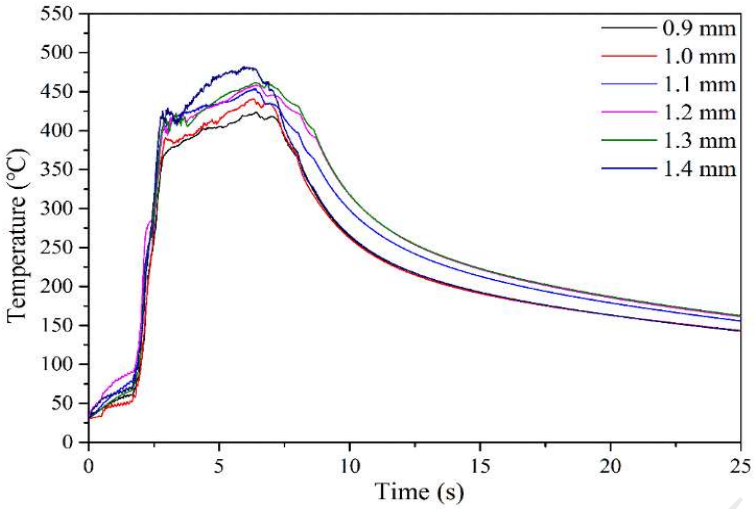

Fig. 9. Thermal cycle at the Al 5754/AlSi coated steel interface during the joining process.

3.3.2. Interfacial microstructure

As shown in Fig. 10(a), defect-free Al 5754/AlSi coated steel weld was successfully manufactured by refill FSSW. The top Al 5754 was imposed onto the AlSi coatings as a result of the frictional heat and axial force imposed by the welding tool, whose microstructure has been extensively investigated elsewhere [40]. Magnified views of blue rectangle at weld center and the red rectangle at the weld boundary are shown in Fig. 10(b) and (c), respectively. In Fig. 10(a) and (b), the Al/steel interface was uniform, with no detection of macro defects at weld center. The original coating interface between the top Al 5754 and AlSi coating could not be identified since the two materials were mixed completely by a combination of mechanical stirring and solid interdiffusion. However, weld imperfection of partial metallurgical bonding or kissing bond was observed at the weld boundary [40, 62], which originated from the original interface between Al 5754 and AlSi coating layer and arrested at the AlSi/IMC layer interface. It is believed that formation of kissing bond was associated with insufficient frictional heat and plastic deformation, thereby the surface oxide film could not be completely broken into particles, thus allowing formation of an intimate metallurgical bonding. The presence of kissing bond is detrimental to the weld strength since it decreases the effective bonded area and acts as a crack initiation and propagation site. Hardness distribution of top Al 5754 measured in midthickness is shown in Fig. 5. Significant softening had not observed in the weld zone when comparing against the hardness of the base material (marked by black dash-dotted line), and it is because that Al 5754 is not a heat treatable

material.

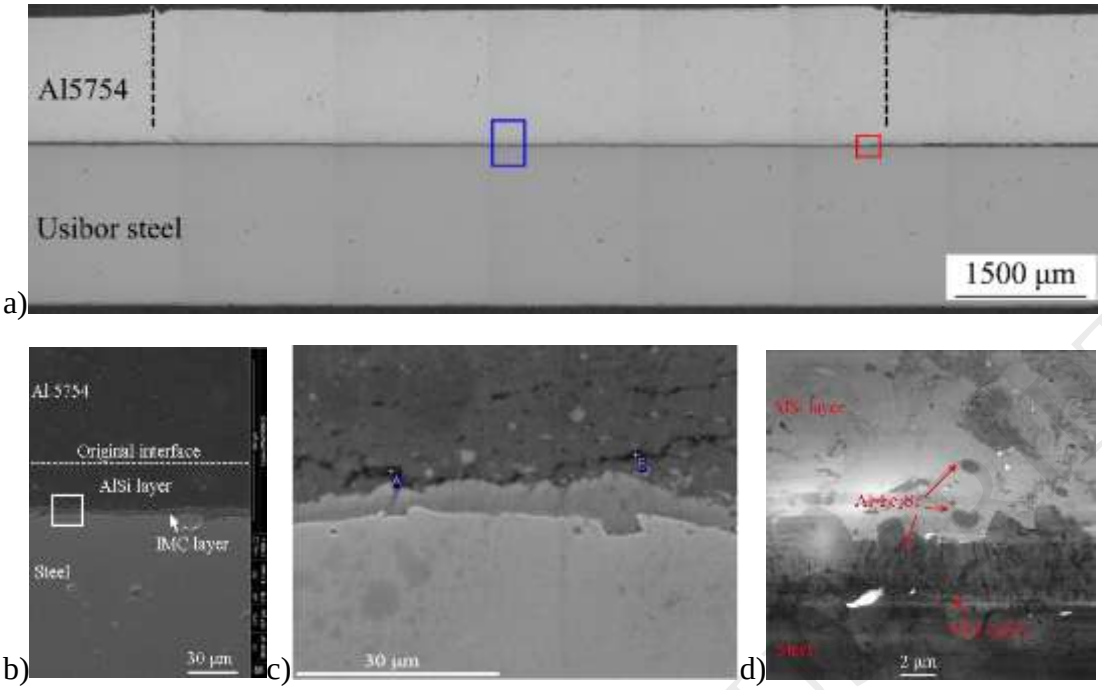

Fig. 10. (a) Optical microscope of the cross-section of Al5754/Al-Si coated weld (1.4 mm penetration depth) and magnified views of the (b) blue rectangle and (c) red rectangle in (a), (d) magnified view of red rectangle in (b).

The maximum temperature shown in Fig. 9 did not exceed both solidus temperature of Al 5754 and eutectic temperature of AlSi coated material (577℃). The results suggested that a real solid-state process had been taken place when joining Al 5754 sheet material to AlSi coated steel. The magnified view of white rectangle in Fig. 10(b) was shown in Fig. 10(d), AlSi coating layer was well bonded to IMC layer and Al 5754 sheet materials. However, poles were noted at the IMC layer/steel substrate interface, which could be formed during the hot-dipping process. Fig. 11 shows a higher magnification at the IMC layer/steel interface, where concentration of Si permeated into the IMC layer. As indicated in Fig. 11 and Table. 3, chemical composition at regions of X and XII is consistent with that of Al_7Fe_2Si and $Al_5Fe_2(Si)$, respectively. Considering that melting point of Al_7Fe_2Si and $Al_5Fe_2(Si)$ is 855 ℃ and 1030 ℃, respectively [63, 64], the joining process had not involved with activities of phase transformation. As shown in Fig. 12, the Al_7Fe_2Si phase is in a finger-like appearance with a [2 -2 1] zone axis, and the $Al_5Fe_2(Si)$ was indexed as a [-1 3 4] zone axis.

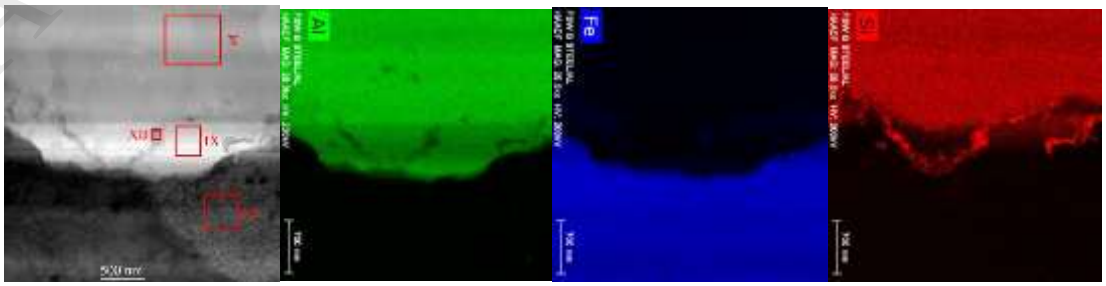

Fig. 11. HAADF image at IMC layer/steel interface with element maps of Al, Fe and Si.

Table. 3. EDX quantification results (wt%) indicated in Fig. 11(a).

	IX	X	XI	XII
Al	46.13	54.8	0.34	26.3
Fe	51.28	36.9	98.51	14
Si	2.57	8.29	1.15	59.7

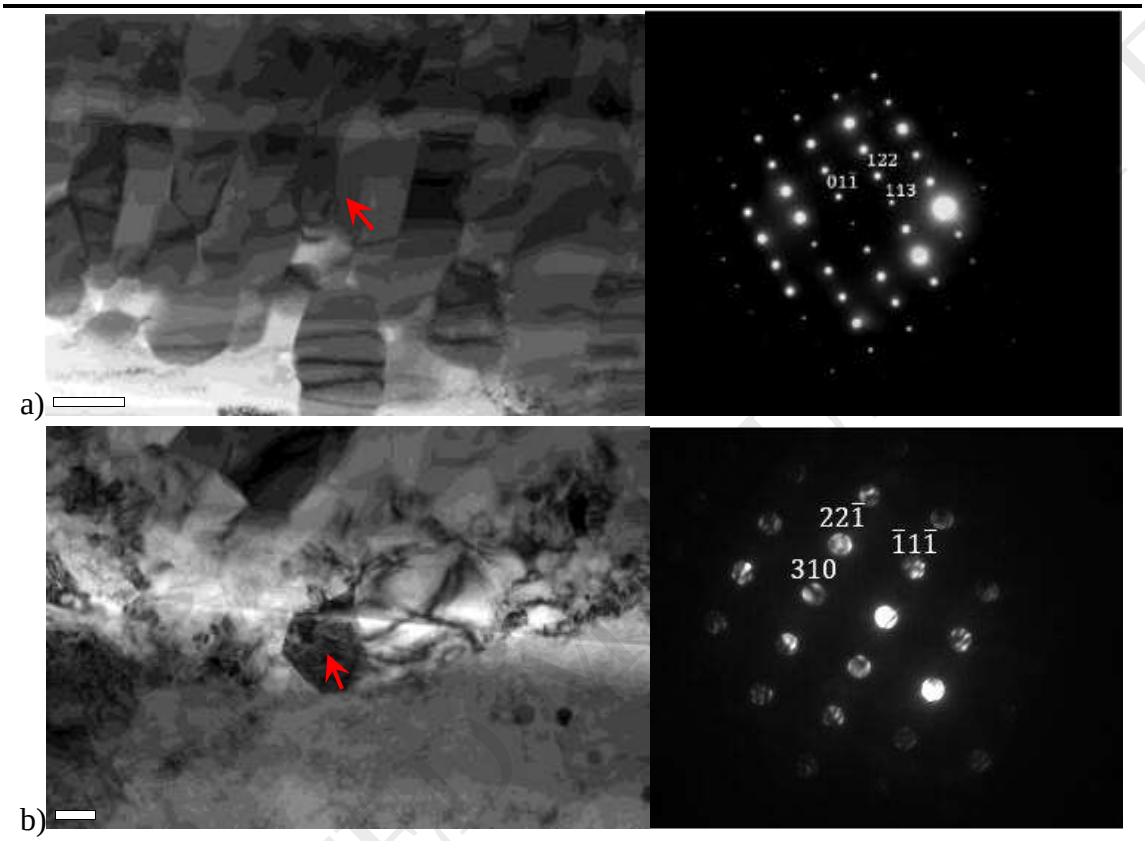

Fig. 12. Bright field images (TEM) and corresponding SAD patterns of selected areas at (a) Al_7Fe_2Si and (b) $Al_5Fe_2(Si)$.

3.4. Mechanical properties of Al/coated steel welds

Findings of previous studies demonstrated that a maximum lap shear strength of 6.95 kN could be achieved for Al/zinc coated steel welds, with welds failed at the Al/steel interface under the lap shear loading [39]. Fig. 13(a) presents a typical interfacial fracture surface on the Al side, and quantification of the chemical composition of regions A–F is in Table. 4. Corresponding fracture path at different locations and quantification of chemical composition in regions I-IX is shown in Fig. 14 and Table. 5, respectively. As shown in Fig. 13(a), the interfacial bonded area is larger than that of the sleeve diameter (indicated by black dash-dotted line), since the zinc coated material was displaced approx. 1 mm outside the sleeve periphery. The displaced zinc coated material reacted with Al material, and created a brazing effect and thus significantly increased the weld strength [39]. As shown in Figs. 13(b),14(a)

and Tables. 4, 5, the crack initiated at the weld boundary and then propagated along the Al-Zn eutectic structure layer around the weld. In subsequent, the crack propagated along the IMC layer in sleeve stirring zone (regions C and D in Fig. 13(a), regions IV-VI in Fig. 14(b)), and thereafter fractured along the Al-Zn eutectic layer in the pin diameter zone (regions A and B in Fig. 13(a), regions VII-IX in Fig. 14(c)). Therefore, the interfacial bonded area can be divided into three categories: i) brazing area, ii) sleeve stirring area and iii) pin stirring area.

a) 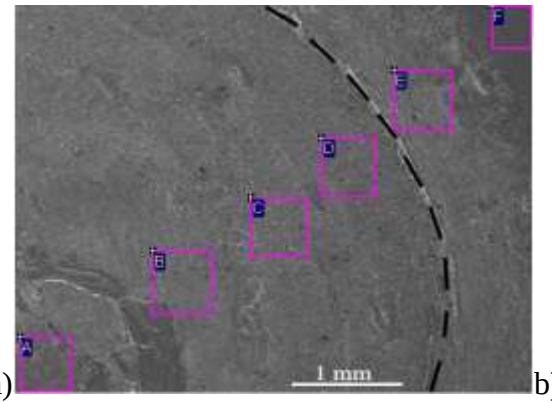

b) 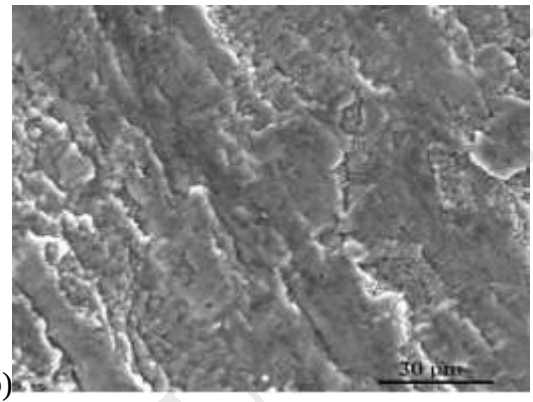

Fig. 13. (a) Overall fracture surface of Al/zinc coated steel weld, (b) magnified view of region E in (a).

Table. 4. EDX quantification results (wt%) indicated in Fig. 13.

	A	B	C	D	E	F
Fe		0.63	28.34	41.39	1.30	
Al	50.88	52.89	46.10	43.85	56.06	100.00
Zn	48.94	45.83	25.05	13.49	42.43	
Si	0.17	0.65	0.51	1.27	0.21	

a) 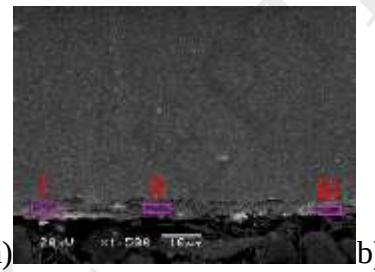
b) 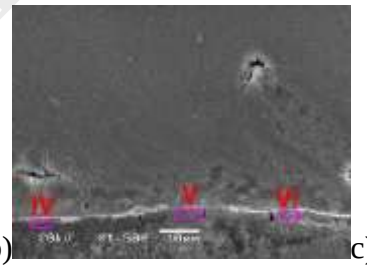
c) 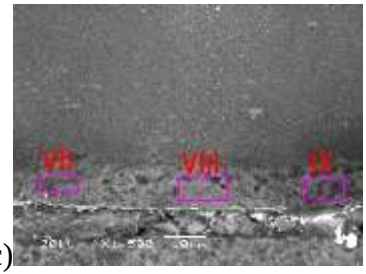

Fig. 14. Fracture path at the location of (a) brazing area, (b) sleeve stirring area and (c) pin stirring area in Fig. 13.

Table. 5. EDX quantification results (wt%) indicated in Fig. 14.

`	I	II	III	IV	V	VI	VII	VIII	IX
Fe	3.13	4.74	2.91	56.41	14.57	17.26			
Al	62.01	61.59	46.41	31.68	71.45	73.52	66.9	58.52	62.61

Zn	34.86	33.67	50.68	10.99	10.9	7.89	33.1	41.2	36.83
Si				0.92	3.08	1.33		0.28	0.56

In Fig. 15, it was found that lap shear strength of Al 5754/AlSi coated steel weld had significant increase when tool penetration depth increased from 0.9 mm to 1.0 mm, and then steady increased, as the tool penetration depth increased from 1.1 mm to 1.4 mm, to a maximum strength of 4.44 kN, which it exceeded the recommended minimum weld strength requirement of 3.79 kN according to the AWS D8.1M:2007 standard (indicated by red dash dotted line) [65]. It is worth mentioning that the reported lap shear strength in present study shows a higher repeatability than previous research literatures as a dwelling period had been considered [40]. Furthermore, weld strength of Al 5754/AlSi coated steel weld showed less sensitivity to welding parameters of this study comparing to Al/zinc coated steel weld [39], this is probably because that melting of base metals or AlSi coated material was not carried out in this study.

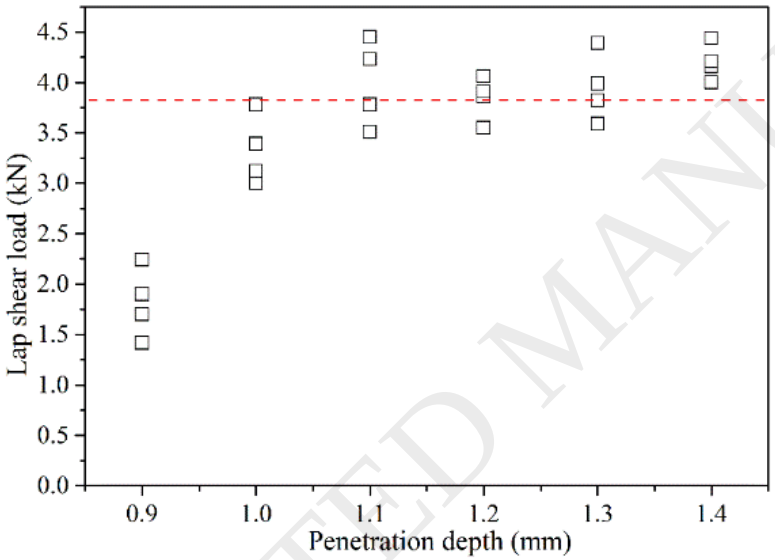

Fig. 15. Effects of tool penetration depth on weld lap shear strength.

Figs. 16-19 show fracture surfaces and paths of Al 5754/AlSi coated steel welds produced at tool sleeve penetrations depth of 0.9 and 1.4 mm, respectively, which with no brazing effect is shown at welds interfaces compared to Al/zinc coated steel weld (Fig. 13). Full interfacial bonding was formed under all penetration depths due to contribution of a dwell period, whose area is consistent with tool sleeve diameter. As shown in Figs. 16-19 and Tables 6-9, the crack initiated at the kissing bond at weld boundary (region D in Fig. 16(a), regions I-III in Fig. 17(a), region E in Fig. 18(a), and regions I-III in Fig. 19(a)), then predominately propagated along the Al 5754/AlSi coating interface when the weld was fabricated under a lower penetration depth (see region B and C in Fig. 16(a)), which suggests that the bonding quality was poor between the Al 5754 and AlSi coating due to the insufficient temperature. In the end, the crack fractured at the AlSi coating/IMC layer interface at the weld center (region A in Fig. 16(a), and regions IV-VI in Fig. 17(b)). However, given that the crack was

more pronounced propagated along the IMC layer after it initiated at the kissing bond (regions A-D in Fig. 18(a), and regions IV-VI in Fig. 19(b)), when the weld was fabricated under a higher penetration depth (1.4 mm), preferable bonding could had been formed at Al 5754/AlSi coating interface and harder IMC layer is believed to be beneficial to the weld strength.

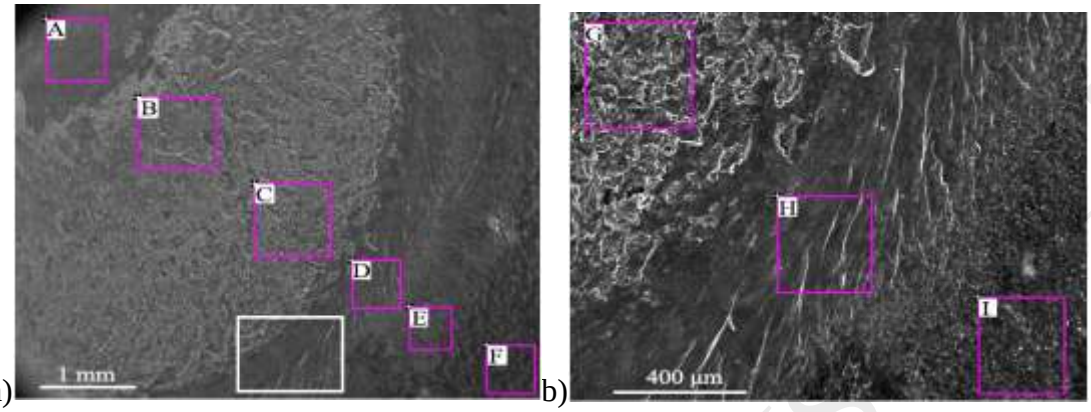

a) b)

Fig. 16. Fracture surface of the Al5754/AlSi coated steel weld: (a) overall and (b) magnified view in the white rectangle in a (0.9 mm penetration, 1.42 kN).

Table. 6. EDX quantification results (wt%) indicated in Fig. 16.

Region	A	B	C	D	E	F	G	H	I
Al	53.65	95.86	95.99	92.66	93.58	92.93	95.14	93.76	95.15
Fe	38.23	1.07	0.72	0.59	1.79	0.83	1.07	0.42	0.45
Si	8.12	2.26	2.38	4.91	2.80	4.15	2.60	4.23	2.50
Mg		0.81	0.91	1.84	1.83	2.09	1.19	1.59	1.90

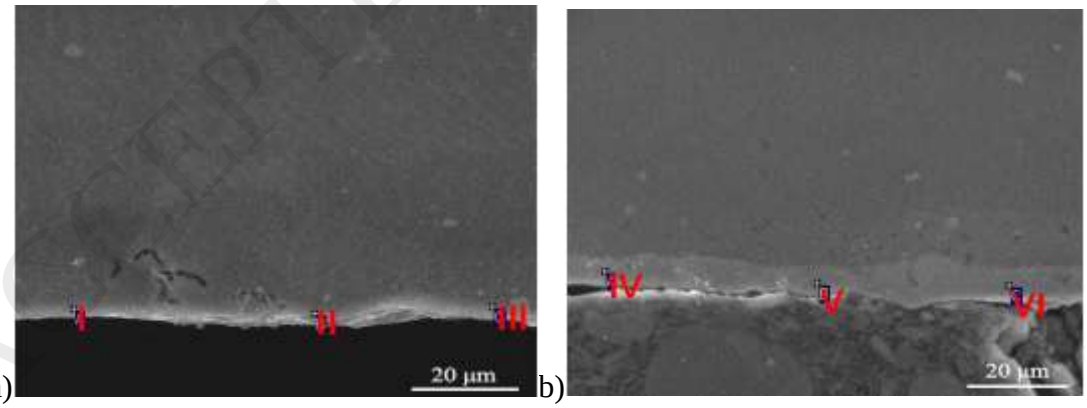

a) b)

Fig. 17. Fracture path at the location of (a) weld boundary and (b) center in Fig. 16(a).

Table. 7. EDX quantification results (wt%) indicated in Fig. 17.

	I	II	III	IV	V	VI
Al	97.52	96.74	97.34	56.32	56.70	53.20
Fe	1.64	0.69	0.29	32.13	32.31	36.21
Si	0.26	0.36		11.55	10.98	10.59
Mg	0.57	2.22	2.37			

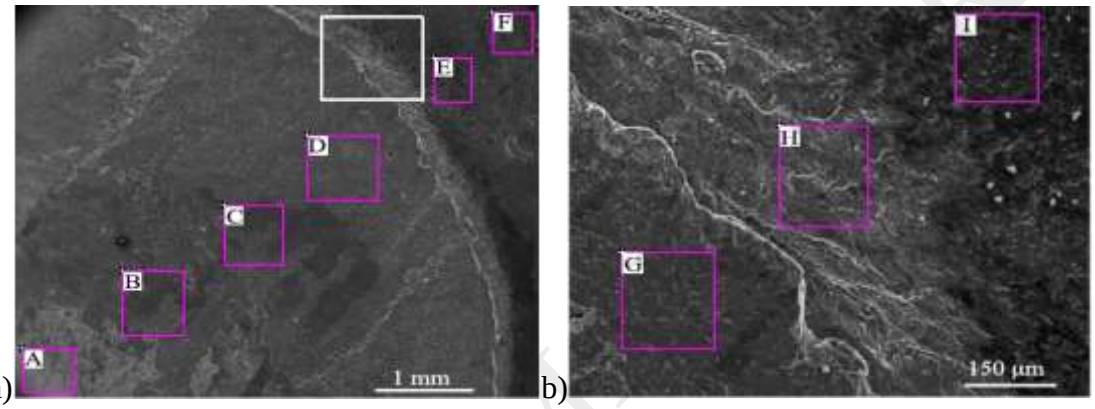

Fig. 18. Fracture surface of the Al5754/AlSi coated steel weld: (a) overall and (b) magnified view in the white rectangle in a (1.4 mm penetration, 4.44 kN).

Table. 8. EDX quantification results (wt%) indicated in Fig. 18.

Region	A	B	C	D	E	F	G	H	I
Al	93.5	54.0	51.7	51.7	96.7	96.4	51.9	95.0	95.8
Fe	2.8	38.2	40.6	40.5		0.1	40.9	0.6	0.6
Si	3.7	7.8	7.7	7.8	1.1	1.3	7.1	3.1	1.6
Mg					2.2	2.2	0.1	1.3	2.0

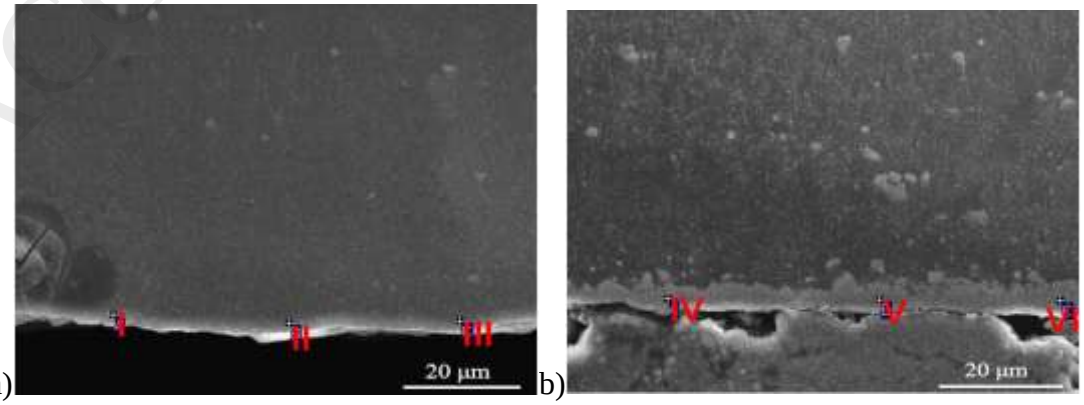

Fig. 19. Fracture path at the location of (a) weld boundary and (b) center in Fig. 18(a).

Table. 9. EDX quantification results (wt%) indicated in Fig. 19.

	I	II	III	IV	V	VI
Al	94.53	93.02	96.41	54.80	54.54	54.52
Fe	3.60	4.00	2.17	32.70	33.84	33.44
Si	0.92	1.58		12.50	11.62	12.04
Mg	0.95	1.40	1.42			

4. Conclusions

In this study, refill friction stir spot welding was used to join Al alloy to uncoated, zinc coated and AlSi coated steels, respectively. Effect of coated materials on the joining mechanism and interfacial microstructure were studied. The following conclusions can be drawn:

(1) Defect-free Al 6022/zinc coated steel weld was successfully fabricated by refill friction stir spot welding. However, Al 6022 and uncoated steel could not be welded under the same welding condition. Al-Zn eutectic structure layer was produced at the Al 6022/zinc coated steel weld interface and a brazing effect was generated outside the sleeve periphery.

(2) Interfacial bonding of Al6022/zinc coated steel weld was attributed to a liquid/solid reaction between the Al-Zn layer and the surrounding materials. Sub-grain boundary was noted in the Al-Zn eutectic structure, and the Al 6022 material directly above the Al-Zn layer underwent insufficient dynamic recrystallization.

(3) Bonding formation at Al 5754 and AlSi coated steel interface was suggested to be induced by a solid/solid reaction between Al alloy and AlSi coating material, as the joining process did not involve with melting of base metals or AlSi coating materials

(4) Kissing bond formed at the weld boundary acted as a crack initiation and propagation site, and the present study showed that weld strength of Al 5754/AlSi coated steel was greatly influenced by properties of original IMC layer.

Acknowledgments

This work has been supported by the Natural Science and Engineering Council (NSERC) of Canada, the Canadian Foundation for Innovation.

References

[1] K. Martinsen, S. Hu, B. Carlson, CIRP Annals-Manufacturing Technology 64(2) (2015) 679-699.

[2] Y. Abe, T. Kato, K. Mori, Joinability of aluminium alloy and mild steel sheets by self piercing rivet, J. Mater. Process. Technol. 177(1) (2006) 417-421.

[3] C.J. Lee, J.Y. Kim, S.K. Lee, D.C. Ko, B.M. Kim, Parametric study on mechanical clinching process for joining aluminum alloy and high-strength steel sheets, J. Mech. Sci. Technol. 24(1) (2010) 123-126.
[4] R. Qiu, H. Shi, K. Zhang, Y. Tu, C. Iwamoto, S. Satonaka, Interfacial characterization of joint between mild steel and aluminum alloy welded by resistance spot welding, Mater. Charact. 61(7) (2010) 684-688.
[5] Z. Shen, Y. Chen, M. Haghshenas, A. Gerlich, Role of welding parameters on interfacial bonding in dissimilar steel/aluminum friction stir welds, Eng. Sci. Technol. 18(2) (2015) 270-277.
[6] E. Taban, J.E. Gould, J.C. Lippold, Dissimilar friction welding of 6061-T6 aluminum and AISI 1018 steel: Properties and microstructural characterization, Mater. Des. 31(5) (2010) 2305-2311.
[7] J. Chen, J. Li, B.S. Amirkhiz, J. Liang, R. Zhang, Formation of nanometer scale intermetallic phase at interface of aluminum-to-steel spot joint by welding–brazing process, Mater. Lett. 137 (2014) 120-123.
[8] M. Thomä, G. Wagner, B. Straß, B. Wolter, S. Benfer, W. Fürbeth, Ultrasound enhanced friction stir welding of aluminum and steel: Process and properties of EN AW 6061/DC04-Joints, J. Mater. Sci. Technol. 34 (2018) 163-172.
[9] L. Agudo, D. Eyidi, C.H. Schmaranzer, E. Arenholz, N. Jank, J. Bruckner, A.R. Pyzalla, Intermetallic FexAly-phases in a steel/Al-alloy fusion weld, J. Mater. Sci. 42(12) (2007) 4205-4214.
[10] V. Patel, S. Bhole, D. Chen, Ultrasonic spot welding of aluminum to high-strength low-alloy steel: microstructure, tensile and fatigue properties, Metall. Mater. Trans. A 45(4) (2014) 2055-2066.
[11] E. Fereiduni, M. Movahedi, A. Kokabi, Aluminum/steel joints made by an alternative friction stir spot welding process, J. Mater. Process. Technol. 224 (2015) 1-10.
[12] Y. Uematsu, T. Kakiuchi, Y. Tozaki, H. Kojin, Comparative study of fatigue behaviour in dissimilar Al alloy/steel and Mg alloy/steel friction stir spot welds fabricated by scroll grooved tool without probe, Sci. Technol. Weld. Join. 17(5) (2012) 348-356.
[13] C.Y. Lee, D.H. Choi, Y.M. Yeon, S.B. Jung, Dissimilar friction stir spot welding of low carbon steel and Al–Mg alloy by formation of IMCs, Sci. Technol. Weld. Join. 14(3) (2009) 216-220.
[14] E. Fereiduni, M. Movahedi, A.H. Kokabi, H. Najafi, Effect of Dwell Time on Joint Interface Microstructure and Strength of Dissimilar Friction Stir Spot-Welded Al-5083 and St-12 Alloy Sheets, Metall. Mater. Trans. A 48(4) (2017) 1744-1758.
[15] J.M. Piccini, H.G. Svoboda, Effect of pin length on Friction Stir Spot Welding (FSSW) of dissimilar Aluminum-Steel joints, Proc. Mater. Sci. 9 (2015) 504-513.
[16] Y. Sun, H. Fujii, N. Takaki, Y. Okitsu, Microstructure and mechanical properties of dissimilar Al alloy/steel joints prepared by a flat spot friction stir welding technique, Mater. Des. 47 (2013) 350-357.
[17] S. Bozzi, A. Helbert-Etter, T. Baudin, B. Criqui, J. Kerbiguet, Intermetallic compounds in Al 6016/IF-steel friction stir spot welds, Mater. Sci. Eng. A 527(16) (2010) 4505-4509.
[18] T. Liyanage, J. Kilbourne, A. Gerlich, T. North, Joint formation in dissimilar Al alloy/steel and Mg alloy/steel friction stir spot welds, Science and Technology of Welding and Joining 14(6) (2009) 500-508.
[19] A. Da Silva, E. Aldanondo, P. Alvarez, E. Arruti, A. Echeverria, Friction stir spot welding of

AA 1050 Al alloy and hot stamped boron steel (22MnB5), Sci. Technol. Weld. Join. 15(8) (2010) 682-687.
[20] Y. Chen, A. Gholinia, P. Prangnell, Interface structure and bonding in abrasion circle friction stir spot welding: a novel approach for rapid welding aluminium alloy to steel automotive sheet, Mater. Chem. Phys. 134(1) (2012) 459-463.
[21] G. Figner, R. Vallant, T. Weinberger, H. Schrottner, H. Pasic, N. Enzinger, Friction stir spot welds between aluminium and steel automotive sheets: influence of welding parameters on mechanical properties and microstructure, Welding in the World 53(1-2) (2009) R13-R23.
[22] K. Chen, X. Liu, J. Ni, Keyhole refilled friction stir spot welding of aluminum alloy to advanced high strength steel, J. Mater. Process. Technol. 249 (2017) 452-462.
[23] K. Ohishi, M. Sakamura, K. Ota, H. Fujii, Novel dissimilar spot welding of aluminium alloy and steel sheets by friction stirring: —Friction anchor welding of aluminium alloy and steel—, Weld. Int. 30(2) (2016) 91-97.
[24] V.-X. Tran, J. Pan, Fatigue behavior of dissimilar spot friction welds in lap-shear and cross-tension specimens of aluminum and steel sheets, Int. J. fatigue 32(7) (2010) 1167-1179.
[25] I. Ibrahim, Y. Uematsu, T. Kakiuchi, Y. Tozaki, Y. Mizutani, Fatigue behaviour of dissimilar Al alloy/galvanised steel friction stir spot welds fabricated by scroll grooved tool without probe, Sci. Technol. Weld. Join. 20(8) (2015) 670-678.
[26] K. Feng, M. Watanabe, S. Kumai, Microstructure and joint strength of friction stir spot welded 6022 aluminum alloy sheets and plated steel sheets, Mater. Trans. 52(7) (2011) 1418-1425.
[27] T. Gendo, K. Nishiguchi, M. Asakawa, S. Tanioka, Spot friction welding of aluminum to steel, SAE Technical Paper, 2007.
[28] K. Miyagawa, M. Tsubaki, T. Yasui, M. Fukumoto, Spot welding between aluminium alloy and Zn-coated steel by friction stirring, Weld. Int. 23(9) (2009) 648-653.
[29] G. Padhy, C. Wu, S. Gao, Friction stir based welding and processing technologies-processes, parameters, microstructures and applications: A review, J. Mater. Sci. Technol. 34 (2017) 1-38.
[30] C. Schilling, J. dos Santos, Method and device for joining at least two adjoining work pieces by friction welding, Google Patents, 2004.
[31] Z. Shen, X. Yang, Z. Zhang, L. Cui, Y. Yin, Mechanical properties and failure mechanisms of friction stir spot welds of AA 6061-T4 sheets, Mater. Des. 49 (2013) 181-191.
[32] Z. Shen, X. Yang, S. Yang, Z. Zhang, Y. Yin, Microstructure and mechanical properties of friction spot welded 6061-T4 aluminum alloy, Mater. Des. (1980-2015) 54 (2014) 766-778.
[33] Y. Zhao, C. Wang, J. Li, J. Tan, C. Dong, Local melting mechanism and its effects on mechanical properties of friction spot welded joint for Al-Zn-Mg-Cu alloy, J. Mater. Sci. Technol. 34 (2017) 185-191.
[34] Z. Shen, Y. Ding, O. Gopkalo, B. Diak, A.P. Gerlich, Effects of tool design on the microstructure and mechanical properties of refill friction stir spot welding of dissimilar Al alloys, J. Mater. Process. Technol. 252C (2018) 751-759.
[35] Z. Shen, X. Yang, Z. Zhang, L. Cui, T. Li, Microstructure and failure mechanisms of refill friction stir spot welded 7075-T6 aluminum alloy joints, Mater. Des. 44 (2013) 476-486.
[36] Z. Shen, Y. Chen, J. Hou, X. Yang, A. Gerlich, Influence of processing parameters on microstructure and mechanical performance of refill friction stir spot welded 7075-T6 aluminium alloy, Sci. Technol. Weld. Join. 20(1) (2015) 48-57.
[37] A.M. Nasiri, Z. Shen, J.S.C. Hou, A.P. Gerlich, Failure analysis of tool used in refill friction

stir spot welding of Al 2099 alloy, Eng. Failure Anal. 84 (2018) 25-33.
[38] Y. Chen, J. Chen, B. Shalchi Amirkhiz, M. Worswick, A. Gerlich, Microstructures and properties of Mg alloy/DP600 steel dissimilar refill friction stir spot welds, Sci. Technol.Weld. Join. 20(6) (2015) 494-501.
[39] Z. Shen, J. Chen, Y. Ding, J. Hou, B.S. Amirkhiz, K. Chan, A. Gerlich, Role of interfacial reaction on the mechanical performance of Al/steel dissimilar refill friction stir spot welds, Sci. Technol. Weld. Join. 23 (2018) 462-477.
[40] Y. Ding, Z. Shen, A. Gerlich, Refill friction stir spot welding of dissimilar aluminum alloy and AlSi coated steel, J. Manuf. Process. 30 (2017) 353-360.
[41] Z. Shen, J. Hou, K. Chan, N. Scotchmer, N. Zhou, A. Gerlich, Spot Welding Aluminum 6022-T4 to Galvanized DP600 sheet by Refill Friction Stir Spot Welding, SWMC XVII conference, Detroit, USA, October, 20th, 2016.
[42] H. Dong, S. Chen, Y. Song, X. Guo, X. Zhang, Z. Sun, Refilled friction stir spot welding of aluminum alloy to galvanized steel sheets, Mater. Des. 94 (2016) 457-466.
[43] S. Fukada, R. Ohashi, M. Fujimoto, H. Okada, Refill friction stir spot welding of dissimilar materials consisting of A6061 and hot dip zinc-coated steel sheets, Proceedings of the 1st International Joint Symposium on Joining and Welding: Osaka, Japan, 6-8 November 2013, Woodhead Publishing, 2014, p. 183.
[44] U. Suhuddin, V. Fischer, A. Kostka, J. dos Santos, Microstructure evolution in refill friction stir spot weld of a dissimilar Al–Mg alloy to Zn-coated steel, Sci. Technol. Weld. Join. 22 (2018) 658-665.
[45] Y. Wang, B. Al-Zubaidy, P.B. Prangnell, The Effectiveness of Al-Si Coatings for Preventing Interfacial Reaction in Al-Mg Dissimilar Metal Welding, Metall. Mater. Trans. A 49(1) (2018) 162-176.
[46] Z. Shen, Y. Ding, J. Chen, A. Gerlich, Comparison of fatigue behavior in Mg/Mg similar and Mg/steel dissimilar refill friction stir spot welds, Int. J. Fatigue 92 (2016) 78-86.
[47] T.B. Massalski, H. Okamoto, P. Subramanian, L. Kacprzak, W.W. Scott, Binary alloy phase diagrams, American Society for Metals, Metals Park, OH, 1986.
[48] Y. Chen, T. Komazaki, T. Tsumura, K. Nakata, Role of zinc coat in friction stir lap welding Al and zinc coated steel, Mater. Sci. Technol. 24(1) (2008) 33-39.
[49] A. Marder, The metallurgy of zinc-coated steel, Prog. Mater. Sci. 45(3) (2000) 191-271.
[50] R. Richards, R. Jones, P. Clements, H. Clarke, Metallurgy of continuous hot dip aluminizing, Int. Mater. Rev. 39(5) (1994) 191-212.
[51] J. Mackowiak, N. Short, Metallurgy of galvanized coatings, Int. Metals Rev. 24(1) (1979) 1-19.
[52] W.J. Cheng, C.J. Wang, Effect of silicon on the formation of intermetallic phases in aluminide coating on mild steel, Intermetallics 19(10) (2011) 1455-1460.
[53] A. Bahadur, Structural studies of hot dip aluminized coatings on mild steel, Mater. Trans. JIM 32(11) (1991) 1053-1061.
[54] X. Liu, B. Diak, TEM Precipitate Identification in Artificial Aged 6022-T4 Alloy and 7075 Artificial Ageing at near Welding Temperature, Report to Ford, 2016.
[55] AWS D 17.2. Specification for resistance welding for aerospace applications, American Welding Society, 2007.
[56] H. Springer, A. Kostka, E. Payton, D. Raabe, A. Kaysser-Pyzalla, G. Eggeler, On the

formation and growth of intermetallic phases during interdiffusion between low-carbon steel and aluminum alloys, Acta Mater. 59(4) (2011) 1586-1600.
[57] H. Springer, A. Szczepaniak, D. Raabe, On the role of zinc on the formation and growth of intermetallic phases during interdiffusion between steel and aluminium alloys, Acta Mater. 96 (2015) 203-211.
[58] P. Su, A. Gerlich, T. North, G. Bendzsak, Energy utilisation and generation during friction stir spot welding, Sci. Technol. Weld. Join. 11(2) (2006) 163-169.
[59] M. Reimann, J. Goebel, T.M. Gartner, J.F. dos Santos, Refilling termination hole in AA 2198–T851 by refill friction stir spot welding, J. Mater. Process.g Technol. 245 (2017) 157-166.
[60] A. Gerlich, P. Su, M. Yamamoto, T.H. North, Effect of welding parameters on the strain rate and microstructure of friction stir spot welded 2024 aluminum alloy, J. Mater. Sci. 42(14) (2007) 5589-5601.
[61] A. Gerlich, M. Yamamoto, T.H. North, Local melting and tool slippage during friction stir spot welding of Al-alloys, J. Mater. Sci. 43(1) (2008) 2-11.
[62] A. Oosterkamp, L.D. Oosterkamp, A. Nordeide, Kissing bond'phenomena in solid-state welds of aluminum alloys, WELDING JOURNAL-NEW YORK- 83(8) (2004) 225-S.
[63] T. Maitra, S. Gupta, Intermetallic compound formation in Fe–Al–Si ternary system: Part II, Mater. Charact. 49(4) (2002) 293-311.
[64] G. Gautam, Aluminium− Iron− Silicon, G. Petzow, G. Effenberg (Eds.), 2005, pp. 394-438.
[65] Specification for Automotive Weld Quality— Resistance Spot Welding of Steel, An American National Standard, 2007.